

Three Artificial Spintronic Leaky Integrate-and-Fire Neurons

Wesley H. Brigner^a, Xuan Hu^a, Naimul Hassan^a, Lucian Jiang-Wei^a, Christopher H. Bennett^b, Felipe Garcia-Sanchez^{c,d}, Otitoaleke Akinola^e, Massimo Pasquale^c, Matthew J. Marinella^b, Jean Anne C. Incorvia^c, Joseph S. Friedman^{a,*}

^a*Electrical and Computer Engineering, University of Texas at Dallas, 800 W Campbell Road
Richardson, Texas 75080, United States*

^b*Sandia National Laboratories, 1515 Eubank Blvd SE
Albuquerque, New Mexico 87185, United States*

^c*Istituto Nazionale di Ricerca Metrologica, Strada delle Cacce, 91
10135 Torino, Italy*

^d*Departamento de Fisica Aplicada, Universidad de Salamanca, Plaza de la Merced s/n
37008 Salamanca, Spain*

^e*Electrical and Computer Engineering, University of Texas at Austin, 110 Inner Campus Drive
Austin, Texas 78705, United States*

*Received Day Month Year
Revised Day Month Year*

Due to their non-volatility and intrinsic current integration capabilities, spintronic devices that rely on domain wall (DW) motion through a free ferromagnetic track have garnered significant interest in the field of neuromorphic computing. Although a number of such devices have already been proposed, they require the use of external circuitry to implement several important neuronal behaviors. As such, they are likely to result in either a decrease in energy efficiency, an increase in fabrication complexity, or even both. To resolve this issue, we have proposed three individual neurons that are capable of performing these functionalities without the use of any external circuitry. To implement leaking, the first neuron uses a dipolar coupling field, the second uses an anisotropy gradient, and the third uses shape variations of the DW track.

Keywords: Artificial neuron, leaky integrate-and-fire (LIF) neuron, magnetic domain wall (DW), neural network crossbar, neuromorphic computing, three-terminal magnetic tunnel junction (3T-MTJ)

1. Introduction

Although modern von Neumann computers are capable of efficiently solving problems of immense proportions, they are highly ineffective at solving problems without a structured data set, such as image recognition. In fact, the human brain can significantly outperform computers in terms of both power

efficiency and speed¹⁻³ when solving these problems. According to neuroscientists, this impressive efficiency can be attributed to interactions between neurons and synapses. A neuron is a complex cell consisting of several components – the axons receive input current pulses from other neurons, the soma integrates those pulses and generate output pulses once

*Corresponding Author: joseph.friedman@utdallas.edu

certain conditions are met, and the dendrites feed the output pulses produced by the soma into other neurons. Synapses, on the other hand, are electrically conductive components that connect the dendrites of one neuron to the axons of other neurons.

One of the primary goals in the field of machine learning is to accurately emulate the behavior of these biological systems. Although it is possible to implement this using software on standard computers^{4,5}, this method is highly inefficient, since the hardware was not specifically designed to perform machine learning, and consumes considerably more energy than an actual brain⁶. It is also possible to design machine learning hardware accelerators that use complementary metal oxide semiconductor (CMOS) technology^{2,3}; however, the volatility of these transistors is not ideal for this application, especially due to the memory dependence of many key algorithms. Therefore, researchers have been attempting to develop non-volatile components to implement both synapses and neurons. Numerous devices, including memristors^{7,8}, magnetic skyrmion devices^{9,10}, three terminal magnetic tunnel junctions (3T-MTJs)^{11,12}, and even organic devices¹³, have already been proposed that successfully emulate synaptic behavior. Due to the complex behaviors occurring in the somas of biological neurons, considerably fewer devices have been proposed to replicate neurons; however, these proposed neurons all require external circuitry to implement certain necessary neuronal functions. To resolve this issue, we have developed three separate three-terminal magnetic tunnel junction (3T-MTJ) based neurons that are capable of intrinsically implementing the desired neuronal behavior¹⁴⁻¹⁶. Section 2 provides a background into neural networking and 3T-MTJs, while Sections 3-5 provide detail regarding our three proposed neurons. Section 6 will discuss system implementation and provide an example with handwritten digit recognition, followed by conclusions in Section 7.

2. Background

A hardware-based neural network implemented using emerging technologies requires the devices to be connected in such a fashion as to be compatible with currently existing fabrication methods. This gives rise to the neural network crossbar array, in which

synapses provide weights from one set of neurons to another.

2.1. *Neural network crossbar array*

In an $N \times M$ neural network, N input neurons are connected to the inputs of the horizontal wires (word lines) and M output neurons are connected to the outputs of the vertical wires (bit lines). $N \times M$ electrically conductive synapses form the intersections between the word and bit lines, and their resistance states determine the weighting between the input neurons and the output neurons¹⁷⁻²⁰.

2.2. *Leaky integrate-and-fire neuron*

In order to accurately emulate a biological neuron, researchers have developed what is known as a Leaky Integrate-and-Fire (LIF) neuron, which improved on the previous Integrate-and-Fire neuron⁴. As the name suggests, an LIF neuron should implement three different functionalities – integrating, leaking, and firing. During the integration phase, a neuron integrates a series of input current spikes. This process increases the energy stored in the neuron, which can be represented as a voltage, or even a domain wall (DW) position. When no input current spike is fed into the neuron, it enters the leaking phase, where the stored energy gradually leaks over time. Finally, if the stored energy reaches a certain threshold, the device will fire, releasing all of its stored energy as a single output spike. A secondary functionality that an LIF output neuron should implement is lateral inhibition – if one neuron has integrated more input spikes than the other, it will inhibit the integration process of other neurons. Using this, it is possible to implement a Winner Take All (WTA) system, where one neuron firing for a given data set will reset not only itself, but all other neurons as well. In other words, only one neuron can fire at a time.

2.3. *Three terminal magnetic tunnel junction*

In general, a magnetic tunnel junction (MTJ) consists of a free ferromagnetic layer electrically insulated from a pinned, or fixed, ferromagnetic layer by a tunnel junction. When an external stimulus is applied to the device, the magnetization state of the free ferromagnetic layer is capable of switching between

two states – antiparallel to the fixed layer and parallel to the fixed layer. When the free layer is in the antiparallel state, it polarizes current antiparallel to the fixed layer, which causes the fixed layer to inhibit electron flow. This results in a high resistance state. Similarly, when the free layer is in the parallel state, it polarizes current parallel to the fixed layer. In this case, however, the current is not impeded by the fixed layer, resulting in a low resistance state.

If the free layer of an MTJ is elongated and contains two oppositely magnetized magnetic domains instead of one, the device becomes a three terminal magnetic tunnel junction (3T-MTJ). At the boundary between the two domains exists a domain wall (DW). When a current is passed through the DW track, the DW will shift in the direction opposite to the applied current^{19,20}. By shifting the DW to one side of the track or the other, it is possible to switch the device between the high and low resistance states. Because of their non-volatility, these devices have garnered significant interest for neuromorphic computing and logic²¹⁻²⁴.

3. Intrinsically Leaking 3T-MTJ Device with Dipolar Coupling Field

In most cases, DWs in 3T-MTJ based neurons leak using external circuitry that produces a current to shift the DWs. However, it is possible to use an dipolar coupling field to induce leaking in the device.

3.1. Device Structure

This device is almost identical to a standard 3T-MTJ device. However, as shown in Figure 1, it contains an electrically isolated ferromagnet underneath the DW track that applies a magnetic field to the track.

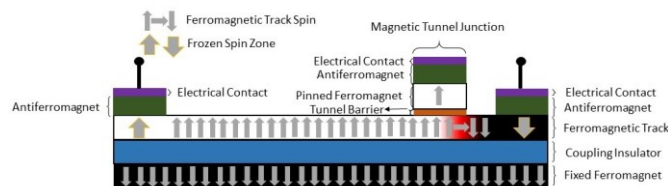


Fig. 1. 3T-MTJ with fixed ferromagnet underneath. The magnetic field applied by the fixed ferromagnet on the bottom will cause the DW (shown in red) to move from right to left.

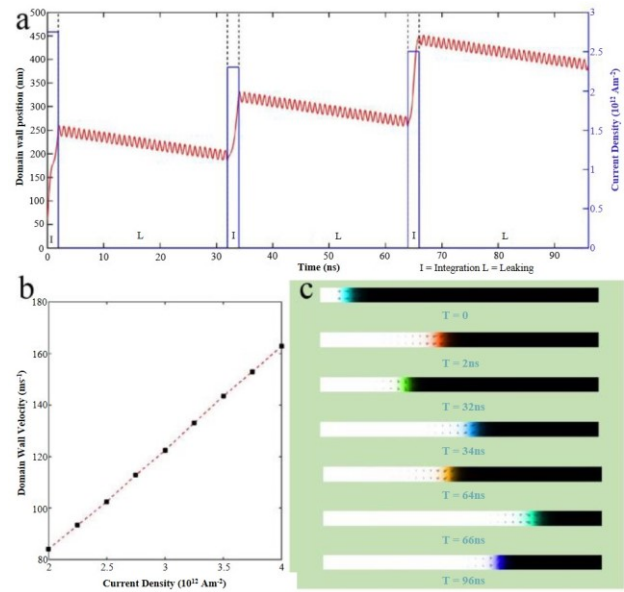


Fig. 2. (a) DW position and current density vs time demonstrating combined integrating and leaking functionalities. Each 2 ns integration period is followed by a 30 ns leaking period where no input is applied resulting in a 96 ns total runtime. (b) Average DW velocity vs current density. As the current density increases, the integration speed increases as well. (c) Snapshots of the micromagnetic simulation for time $t=0$ ns, $t=2$ ns, $t=32$ ns, $t=34$ ns, $t=64$ ns, $t=66$ ns, and $t=96$ ns. Note that the DW magnetization state rotates – this is evidence of DW precession.

The device was simulated using version 3.10 of the micromagnetic simulator mumax3²⁵. The length of the device is 600 nm, the width of the device is 32 nm, and the thickness of the device is 1 nm, while the cell sizes were $1 \times 1 \times 1$ nm³. However, the DW does not have a 600 nm range of motion in the track, since 30-nm-wide antiferromagnets at either end of the track generate regions of frozen spin to prevent the DW from annihilating itself on the edges of the material. This results in a 540 nm range of motion for the DW. Similar to CoFeB, the magnetic saturation M_{sat} is 1 T, the exchange stiffness A_{ex} is 1.3×10^{-11} J/m, the perpendicular anisotropy constant k_{u1} is 4×10^5 J/m³, the non-adiabaticity factor ξ is 0.9, the Landau-Lifshitz-Gilbert damping constant α is 0.015. The polarization of spin-transfer torque is 1; the use of a more practical value would act only as a scaling factor.

3.2. Leaking with dipolar coupling field

When a magnetic field is applied to a magnetic domain in the same direction as the domain's magnetization state, the domain will expand. Conversely, when a magnetic field is applied to a magnetic domain in the direction opposite to the domain's magnetization state, the domain will shrink. Applying a magnetic field to a DW track is a combination of these effects – one of the domains will expand, while the other will shrink. This causes the DW to shift without any external circuitry.

3.3. Combined integrating and leaking with dipolar coupling field

Figure 2 demonstrates the combined integrating and leaking functionalities of the device. A series of three 2 ns current pulses are applied to the DW track, each followed by a 30 ns leaking period where no input is applied to the device.

3.4. Firing through magnetoresistance switching

We assume that the DW will fire whenever it passes underneath the MTJ, switching the resistance from a high-resistance state to a low resistance state. This will produce an output current spike. During the firing process, the DW will also be reset to its original state. For a brief 'refractory' period after firing, the device will not integrate any input current spikes.

4. Intrinsically Leaking 3T-MTJ Device with Graded Anisotropy

4.1. Device structure

Similar to the 3T-MTJ with an dipolar coupling field, the device structure is almost identical to a standard 3T-MTJ. However, instead of a ferromagnet placed underneath the DW track, this device contains an anisotropy gradient²⁶, which can be achieved using a thickness and/or composition gradient²⁷⁻²⁹. The possibility of creating a voltage-induced anisotropy gradient has also been suggested³⁰.

The device has a length L of 250 nm, a width w of 32 nm, and a thickness t of 1.5 nm, while the cell size is $1 \times 1.5 \text{ nm}^2$. This device has 10 nm wide frozen

spin regions, resulting in a 230 nm range of motion for the DW. The exchange stiffness A_{ex} is $1.3 \times 10^{-11} \text{ J/m}$, the Landau-Lifshitz-Gilbert damping constant α is 0.02, the non-adiabaticity of spin transfer torque ξ is 0.2, and the magnetic saturation M_{sat} is $800 \times 10^3 \text{ A/m}$. The lower anisotropy value an_{sl} is $0.5 \times 10^6 \text{ J/m}^3$, and the upper anisotropy value an_{sh} is $5 \times 10^6 \text{ J/m}^3$. In this case, since no external excitation is applied, the dipolar coupling field B_{ext} is 0 T.

4.2. Leaking with graded anisotropy

When a DW exists in a track with a low anisotropy, it is in a lower energy state than if it existed in a track with a stronger magnetocrystalline anisotropy. Therefore, by linearly varying the anisotropy, it is possible to generate an energy landscape that is more favorable to the DW existing on one end of the track than on the other. This causes the DW to shift from the region of higher anisotropy to the region of lower anisotropy without the use of a current or magnetic field.

4.3. Combined integrating and leaking with graded anisotropy

Figure 3 illustrates the combined integration and leaking functionalities of a 3T-MTJ neuron with graded anisotropy. Again, there are three 2 ns current pulses, but each pulse is followed by a 50 ns leaking period.

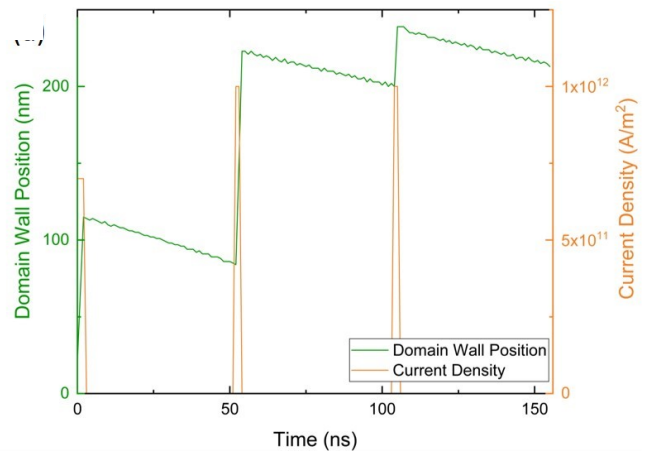


Fig. 3. DW position and current density vs time demonstrating the combined leaking and integrating functionalities of a 3T-MTJ neuron with graded anisotropy. Each 2-ns-wide current pulse is followed by a 50 ns leaking period, resulting in a 156 ns runtime.

4.4. Firing through magnetoresistance switching

The firing mechanism for this neuron is identical to that of the neuron with a dipolar coupling field. Once the DW passes underneath the MTJ, the neuron resets itself and releases an output pulse. This is followed by a brief refractory period.

5. Intrinsically Leaking 3T-MTJ Device with Shape-Based DW Drift

5.1. Device structure

This device is similar to a standard 3T-MTJ; however, instead of having a rectangular x-y cross-section, it has a trapezoidal x-y cross-section. This structure is illustrated in Figure 4.

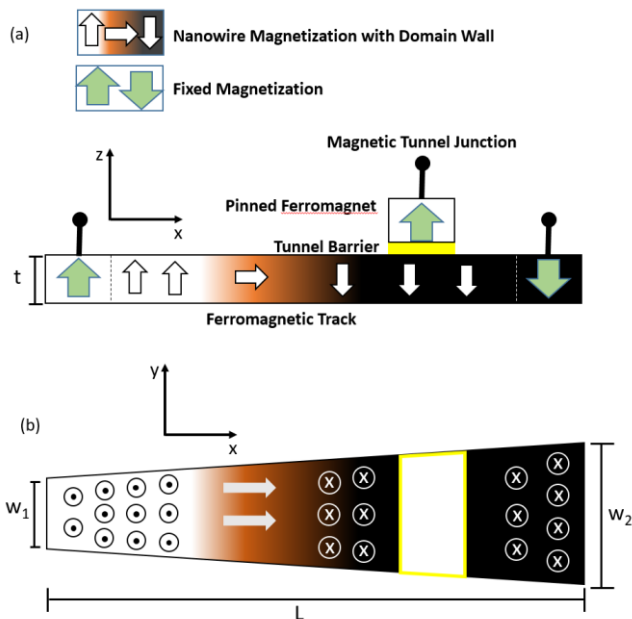


Fig. 4. (a) Side view of the device. (b) Top view of the device, demonstrating the trapezoidal x-y cross-section. The narrow end has width w_1 , while the wide end has width w_2 .

The device has a length L of 250 nm and a thickness t of 1.5 nm, and the left end of the device has width w_1 of 25 nm while the right end of the device has width w_2 of 100 nm. Again, the device has 10-nm-wide frozen spin regions on both sides of the track,

resulting in a DW range of motion of 230 nm. The material parameters represent CoFeB³¹, where the exchange stiffness $A_{ex} = 1.3 \cdot 10^{-11}$ J/m, the Landau-Lifshitz-Gilbert damping constant $\alpha = 0.02$, the non-adiabaticity of spin-transfer torque $\xi = 0.2$, and the magnetic saturation $M_{sat} = 1$ T.

5.2. Leaking with shape-based DW drift

Similar to a DW in a track with graded anisotropy, a DW in a trapezoidal track will exist in a lower energy state in a narrower region of the track and will exist in a higher energy state in a wider region of the track²³. Again, this creates an energy landscape that is favorable to the DW existing at the left end of the track. If the DW is shifted to a wider end of the track using a current, it will begin to shift back to the narrower end after the current is removed.

5.3. Firing through magnetoresistance switching

The firing mechanism for this neuron is identical to that for the neuron with an dipolar coupling field and the neuron with a graded anisotropy. Once the DW passes underneath the MTJ, the neuron resets itself and releases an output pulse. This is followed by a brief refractory period.

6. Lateral Inhibition

6.1. Intrinsically Leaking 3T-MTJ Device with Shape-Based DW Drift

Due to the fact that a 3T-MTJ consists primarily of a ferromagnetic track, it will produce fringe fields to either side. Similar to a ferromagnet placed underneath the track, this can act as an external field for other neurons. If the DW of one neuron exists in a higher energy state than a neighboring neuron, the first neuron's fringe fields will inhibit the second neurons progression. Conversely, if one neuron exists in a lower energy state than a neighboring neuron, the first

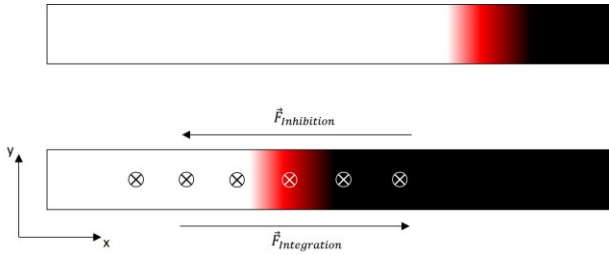


Fig. 5. The fringe field generated by the +z magnetized region (white) in the upper DW is effectively an dipolar coupling field in the $-z$ direction at the lower neuron. This will generally cause the $-z$ region (black) in the lower neuron to expand and the +z region in the lower neuron to shrink, unless the integration force is large enough to overcome the combined inhibition and leaking forces. In turn, the lower neuron will tend to integrate slower than the upper neuron.

neuron will actually promote the second neuron's integration. This effect is illustrated in Figure 5.

An example of lateral inhibition is shown in Figure 6, where two side-by-side neurons receive constant inputs. In the first case, where the upper neuron (neuron 1) receives an input current density of 1.5×10^{12} A/m² and the lower neuron (neuron 2) receives an input current density of 2×10^{12} A/m², neuron 2 is finished integrating by $t = 7.3$ ns, while neuron 1 did not finish. In the second case, neuron 1 receives the same input current density of 1.5×10^{12} A/m², but neuron 2 does not receive any input at all. Here, neuron 1 is finished integrating by $t = 7.3$ ns, while neuron 2 did not integrate due to the lack of an input current.

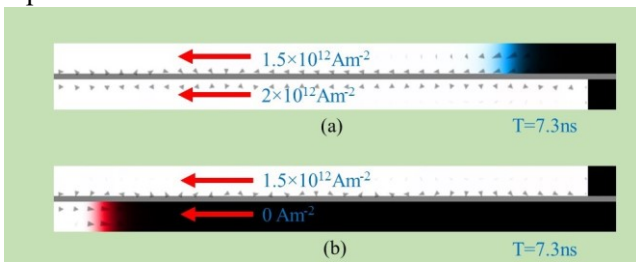


Fig. 6. Demonstration of lateral inhibition. (a) Neuron 2 receives a higher input current than neuron 1, and neuron 1 does not finish integrating by $t = 7.3$ ns. (b) Neuron 2 receives no input current, and neuron 1 finishes integrating by $t = 7.3$ ns.

Figure 7 provides a graphical illustration of this effect. Assuming a constant input current density to neuron 2 of 1.5×10^{12} A/m², increasing the input

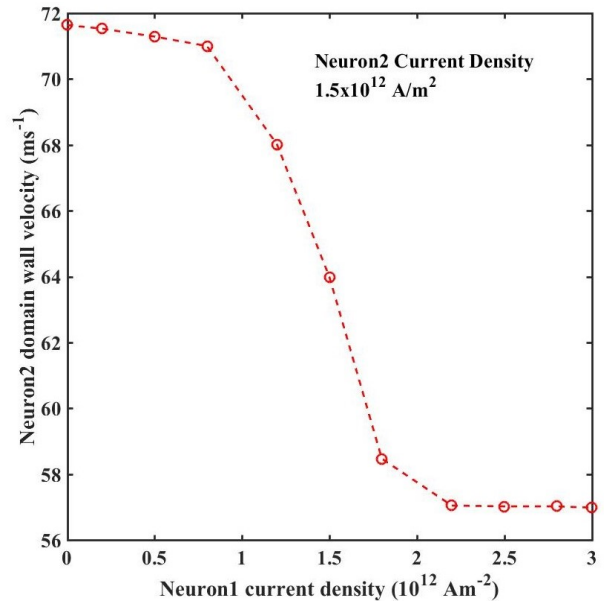


Fig. 7. Neuron 2 velocity vs neuron 1 current density. As the input current density to Neuron 1 increases, the average DW velocity of neuron 2 decreases.

current to neuron 1 decreases the average velocity of neuron 2's DW. Neuron 2's average velocity reaches a lower limit of 57 m/s when neuron 1's input current density reaches $\sim 2.25 \times 10^{12}$ A/m².

6.2. Winner take all using lateral inhibition

By placing multiple neurons next to each other, as in Figure 8, it is possible to implement a winner take all (WTA) system. The neuron that exists in a higher energy state than the other neurons will inhibit the

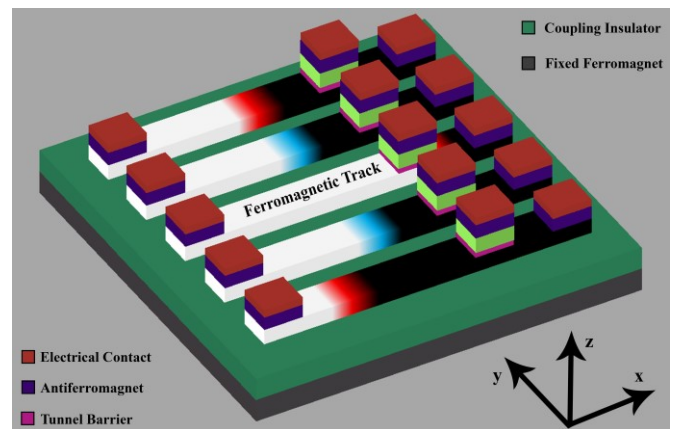


Fig. 8. Illustration of the WTA system, using the neurons discussed in Section 3.

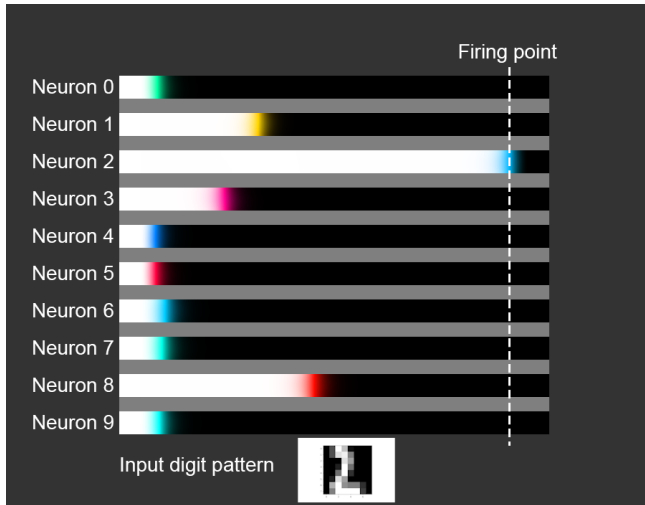


Fig. 9. Illustration of a WTA system with 10 performing pattern recognition on a hand-written digit. In this case, the input was an ‘2’. The first neuron to reach the firing point was neuron 2, indicating that the system correctly identified the digit.

integration of the other neurons and be promoted by the other neurons. Using the combination of the LIF neuron characteristics and lateral inhibition/WTA, it is possible to perform handwritten digit recognition.

Figure 9 provides an example of a WTA system performing handwritten digit recognition using 10 neurons given a pre-trained synaptic crossbar array¹⁴, with each neuron corresponding to a specific digit. If one neuron fires, the system will recognize the input as the digit corresponding to the neuron that fired. For instance, if neuron 2 fires, the system recognizes the input as a ‘2’. Once a neuron fires, all output neurons reset and enter a brief refractory period in which no signals are integrated. The input signals were fed into the system by a pretrained memristor crossbar. This system was capable of recognizing handwritten digits with an accuracy of 94%.

7. Conclusion

This work discusses three previously proposed LIF neurons that are capable of intrinsically providing the leaking, integrating, firing, and lateral inhibition functionalities by making different modifications to a standard 3T-MTJ device, including by applying a magnetic field, introducing a magnetocrystalline anisotropy gradient, and introducing shape variations. These modifications reduce the amount of external circuitry required to replicate neuronal behavior, in

turn allowing for reduced power consumption and ease-of-fabrication. Therefore, these could be important building blocks for future neural networks.

Acknowledgments

This research is sponsored in part by the National Science Foundation under CCF awards #1910800 and #1910997. The authors thank E. Laws, J. McConnell, N. Nazir, L. Philoon, and C. Simmons for technical support, and the Texas Advanced Computing Center at The University of Texas at Austin for providing computational resources.

This paper describes objective technical results and analysis. Any subjective views or opinions that might be expressed in the paper do not necessarily represent the views of the U.S. Department of Energy or the United States Government. Sandia National Laboratories is a multimission laboratory managed and operated by National Technology Engineering Solutions of Sandia, LLC, a wholly owned subsidiary of Honeywell International Inc., for the U.S. Department of Energy’s National Nuclear Security Administration under contract DE-NA0003525.

References

1. Balasubramanian, V., “Heterogeneity and Efficiency in the Brain,” *Proceedings of the IEEE* **103**(8), 1346–1358 (2015).
2. Akopyan, F., Sawada, J., Cassidy, A., Alvarez-Icaza, R., Arthur, J., Merolla, P., Imam, N., Nakamura, Y., Datta, P., et al., “TrueNorth: Design and Tool Flow of a 65 mW 1 Million Neuron Programmable Neurosynaptic Chip,” *IEEE Transactions on Computer-Aided Design of Integrated Circuits and Systems* **34**(10), 1537–1557 (2015).
3. Merolla, P. A., Arthur, J. V., Alvarez-Icaza, R., Cassidy, A. S., Sawada, J., Akopyan, F., Jackson, B. L., Imam, N., Guo, C., et al., “A million spiking-neuron integrated circuit with a scalable communication network and interface,” *Science* **345**(6197), 668–673 (2014).
4. Delorme, A., Gautrais, J., Rullen, R. V., Thorpe, S., “SpikeNET: A simulator for modeling large networks of integrate and fire neurons,” *Neurocomputing* **26-27**, 989–996 (1999).
5. Han, S., Mao, H., Dally, W. J., “Deep Compression: Compressing Deep Neural Networks with Pruning, Trained Quantization, and Huffman Coding,” *ICLR* 2016.
6. Sengupta, B., Stemmler, M. B., “Power Consumption During Neuronal Computation,” *Proceedings of the IEEE* **102**(5), 738–750 (2014).

7. Strukov, D. B., Snider, G. S., Stewart, D. R., Williams, R. S., "The missing memristor found," *Nature* **453**(7191), 80–83 (2008).
8. Querlioz, D., Zhao, W. S., Dollfus, P., Klein, J.-O., Bichler, O., Gamrat, C., "Bioinspired networks with nanoscale memristive devices that combine the unsupervised and supervised learning approaches," *Proceedings of the 2012 IEEE/ACM International Symposium on Nanoscale Architectures (NANOARCH)* 12 (2012).
9. Chen, X., Kang, W., Zhu, D., Zhang, X., Lei, N., Zhang, Y., Zhou, Y., Zhao, W., "A compact skyrmionic leaky-integrate-fire spiking neuron device," *Nanoscale* **10**(13), 6139–6146 (2018).
10. Huang, Yangqi, Wang Kang, Xichao Zhang, Yan Zhou, Weisheng Zhao. "Magnetic skyrmion-based synaptic devices." *Nanotechnology* 28, no. 8 (2017): 08LT02.
11. Dutta, S., Siddiqui, S. A., Buttner, F., Liu, L., Ross, C. A., Baldo, M. A., "A logic-in-memory design with 3-terminal magnetic tunnel junction function evaluators for convolutional neural networks," *2017 IEEE/ACM International Symposium on Nanoscale Architectures (NANOARCH)* (2017).
12. O. Akinola, E. J. Kim, N. Hassan, J. S. Friedman, J. A. C. Incorvia, Neuromorphic Computing with Domain Wall-Based Three-Terminal Magnetic Tunnel Junctions: Synapse, *Joint IEEE International Magnetism Conference & Conference on Magnetism and Magnetic Materials*, Jan. 2019.
13. Y. V. D. Burgt et al., "A non-volatile organic electrochemical device as a low-voltage artificial synapse for neuromorphic computing," *Nature Materials* **16**(4), 414–418 (2017)
14. Hassan, N., Hu, X., Jiang-Wei, L., Brigner, W. H., Akinola, O. G., Garcia-Sanchez, F., Pasquale, M., Bennett, C. H., Incorvia, J. A. C., et al., "Magnetic domain wall neuron with lateral inhibition," *Journal of Applied Physics* **124**(15), 152127 (2018).
15. Brigner, W. H., Hu, X., Hassan, N., Bennett, C. H., Incorvia, J. A. C., Garcia-Sanchez, F., Friedman, J. S., "Graded-Anisotropy-Induced Magnetic Domain Wall Drift for an Artificial Spintronic Leaky Integrate-and-Fire Neuron," *IEEE Journal on Exploratory Solid-State Computational Devices and Circuits*, 1–1 (2019).
16. W. H. Brigner et al., "Shape-based Magnetic Domain Wall Drift for an Artificial Spintronic Leaky Integrate-and-Fire Neuron," *IEEE Transactions on Electron Devices* **66**:11, 4970-4975 (2019).
17. Lin, Y.-P., Bennett, C. H., Cabaret, T., Vodenicarevic, D., Chabi, D., Querlioz, D., Jusselme, B., Derycke, V., Klein, J.-O., "Physical Realization of a Supervised Learning System Built with Organic Memristive Synapses," *Scientific Reports* **6**(1) (2016).
18. C. H. Bennett, J. A. C. Incorvia, X. Hu, N. Hassan, J. S. Friedman, M. M. Marinella, "Semi-Supervised Learning and Inference in Domain-Wall Magnetic Tunnel Junction (DW-MTJ) neural Networks," *Proc. SPIE Spintronics XII*, Aug. 2019 (invited).
19. Sharad, M., Fan, D., Aitken, K., Roy, K., "Energy-Efficient Non-Boolean Computing With Spin Neurons and Resistive Memory," *IEEE Transactions on Nanotechnology* **13**(1), 23–34 (2014).
20. Sharad, M., Fan, D., Aitken, K., Roy, K., "Energy-Efficient Non-Boolean Computing With Spin Neurons and Resistive Memory," *IEEE Transactions on Nanotechnology* **13**(1), 23–34 (2014).
21. Currivan, J. A., Jang, Y., Mascaro, M. D., Baldo, M. A., Ross, C. A., "Low Energy Magnetic Domain Wall Logic in Short, Narrow, Ferromagnetic Wires," *IEEE Magnetics Letters* **3**, 3000104–3000104 (2012).
22. Currivan-Incorvia, J. A., Siddiqui, S., Dutta, S., Evarts, E. R., Ross, C. A., Baldo, M. A., "Spintronic logic circuit and device prototypes utilizing domain walls in ferromagnetic wires with tunnel junction reading," *2015 IEEE International Electron Devices Meeting (IEDM)* (2015).
23. J. S. Friedman and A. V. Sahakian, "Complementary Magnetic Tunnel Junction Logic," *IEEE Transactions on Electron Devices* **61**(4), 1207–1210 (2014)
24. X. Hu, A. Timm, W. H. Brigner, J. A. C. Incorvia, J. S. Friedman, SPICE-Only Model for Spin-Transfer Torque Domain Wall MTJ Logic, *IEEE Transactions on Electron Devices*, 66:6, 2817-2821 (2019).
25. Vansteenkiste, A., Leliaert, J., Dvornik, M., Helsen, M., Garcia-Sanchez, F., Waeyenberge, B. V., "The design and verification of MuMax3," *AIP Advances* **4**(10), 107133 (2014).
26. S. Li et al., "Magnetic skyrmion-based artificial neuron device," *Nanotechnology* **28**(31), 31LT01 (2017).
27. Y. Sun, C. R. Sullivan, W. Li, D. Kopp, F. Johnson, S. T. Taylor, "Soft magnetic properties of obliquely deposited Co–Zr–O films", *IEEE Trans. Magn.*, vol. 43, no. 12, pp. 4060-4063, Dec. 2007.
28. N. N. Phuoc, L. T. Hung, C. K. Ong, "FeCoHfN thin films fabricated by co-sputtering with high resonance frequency", *J. Alloys Compounds*, vol. 509, no. 9, pp. 4010-4013, 2011.
29. S. Li, Z. Huang, J.-G. Duh, M. Yamaguchi, "Ultra-high-frequency ferromagnetic properties of FeCoHf films deposited by gradient sputtering", *Appl. Phys. Lett.*, vol. 92, no. 9, 2008.
30. C. Ma et al., "Electric Field-Induced Creation and Directional Motion of Domain Walls and Skyrmion Bubbles," *Nano Letters* **19**(1), 353-361 (2019).
31. Y. Zhang et al., "Compact Modeling of Perpendicular-Anisotropy CoFeB/MgO Magnetic Tunnel Junctions," *IEEE Transactions on Electron Devices* **59**(3), 819–826 (2012)